Myeloperoxidase targets oxidative host attacks to *Salmonella* and prevents collateral tissue damage

Nura Schürmann[1‡], Pascal Forrer[3‡], Olivier Casse[1], Jiagui Li[1], Boas Felmy[4], Anne-Valérie Burgener[3], Nikolaus Ehrenfeuchter[2], Wolf-Dietrich Hardt[4], Mike Recher[3], Christoph Hess[3], Astrid Tschan-Plessl[3], Nina Khanna[3], Dirk Bumann[1]*

[1]Focal Area Infection Biology, [2]Imaging Core Facility, Biozentrum, [3]Department Biomedicine and University Hospital Basel, University of Basel, CH-4056 Basel; [4]Institute of Microbiology, ETH Zurich, CH-8093 Zurich

‡These authors contributed equally to the work.

Correspondence and requests for materials should be addressed to dirk.bumann@unibas.ch.

Dirk Bumann

Klingelbergstrasse 50/70

CH-4056 Basel

Phone: +41 61 267 2382

Abstract

Host control of infections crucially depends on the capability to kill pathogens with reactive oxygen species (ROS). However, these toxic molecules can also readily damage host components and cause severe immunopathology. Here, we show that neutrophils use their most abundant granule protein, myeloperoxidase, to target ROS specifically to pathogens while minimizing collateral tissue damage. A computational model predicted that myeloperoxidase efficiently scavenges diffusible H_2O_2 at the surface of phagosomal *Salmonella*, and converts it into highly reactive HOCl (bleach), which rapidly damages biomolecules within a radius of less than 0.1 µm. Myeloperoxidase-deficient neutrophils were predicted to accumulate large quantities of H_2O_2 that still effectively kill *Salmonella*, but most H_2O_2 would leak from the phagosome. *Salmonella* stimulation of neutrophils from normal and myeloperoxidase-deficient human donors experimentally confirmed an inverse relationship between myeloperoxidase activity and extracellular H_2O_2 release. Myeloperoxidase-deficient mice infected with *Salmonella* had elevated hydrogen peroxide tissue levels and exacerbated oxidative damage of host lipids and DNA, despite almost normal *Salmonella* control. These data show that myeloperoxidase has a major function in mitigating collateral tissue damage during antimicrobial oxidative bursts, by converting diffusible long-lived H_2O_2 into highly reactive, microbicidal, and locally confined HOCl at pathogen surfaces.

When stimulated by microbes, neutrophils use the enzyme phagocyte NADPH oxidase to generate bursts of superoxide O_2^- that spontaneously dismutates to hydrogen peroxide H_2O_2. The enzyme myeloperoxidase (MPO) can then convert O_2^- and H_2O_2 into hypohalites (predominantly HOCl, bleach; but also HOBr)[1]. The MPO intermediate "compound I" is the strongest two-electron oxidant that is generated in humans[2], and its product HOCl is a kinetically and thermodynamically highly reactive oxidant[3] with potent antimicrobial efficacy[1]. MPO can also contribute to the formation of antimicrobial neutrophil extracellular traps (NETs)[4,5]. However, MPO has apparently an only limited role in infection control in humans and mice, at least in modern hygienic environments, in marked contrast to NADPH oxidase, which is essential for controlling a wide range of infections[1]. MPO has clear detrimental effects in cardiovascular diseases[6], and MPO inhibitors are currently in clinical development for these and other indications[7]. Taken together, it is not entirely clear why neutrophils contain large quantities of MPO.

Results

Computational modeling of MPO impact on *Salmonella* killing and ROS leakage

To re-examine the role of MPO during infection, we combined a previously described computational model of oxidative bursts in neutrophil phagosomes[8], with our recent model of ROS defense in *Salmonella enterica* serovar Typhimurium[9] (Supplementary Note). We used this model to compare conditions in neutrophils with various levels of MPO (Fig. 1).

In absence of MPO (Fig. 1a, left), this model predicted H_2O_2 to be the dominant ROS output (Fig. 1a, b), as previously reported[8,9]. *Salmonella* could detoxify about 3% of this H_2O_2 output using its catalase KatG, while peroxidases (AhpC, Tsa, Tpx) had low saturated activities (Fig. 1c), consistent with the respective enzyme kinetics[10]. This minor detoxification had negligible impact on the *Salmonella* internal H_2O_2 concentration compared to the phagosomal lumen (Fig. 1d), resulting in lethal levels well above the toxicity threshold of about 2 μM[11] suggesting H_2O_2-mediated *Salmonella* killing under conditions without MPO[9]. At the same time, most H_2O_2 would actually not enter *Salmonella*, but rather leak out of the phagosome to the surrounding neutrophil cytosol (Fig. 1b), reflecting diffusion of H_2O_2 through membranes at substantial rates (around 1-3 x 10^{-3} cm s^{-1} across bacterial[11] and mammalian[12] membranes), again in agreement with previous modelling results[8]. By contrast, O_2^- concentration in *Salmonella* compartments remained always at non-toxic sub-nanomolar levels in agreement with our previous results[9].

In presence of low levels of MPO, the model suggested that H_2O_2 was partially converted to HOCl (Fig. 1a, middle; 50% conversion to HOCl at 0.13 mM MPO; Fig. 1b). The remaining H_2O_2 would still overwhelm *Salmonella* detoxification and kill *Salmonella* (Fig. 1d), but also largely leak from the phagosome (Fig. 1b). By contrast, HOCl would act locally. Based on HOCl reaction rate constants[3], its diffusion coefficient[13], and protein concentrations in phagosomes[8], HOCl is expected to have a lifetime of 0.1 μs, and a diffusion length of about 30 nm (similar to previous estimates[8]). This short reach would confine HOCl-mediated damage largely to the phagosome, consistent with recent

57 experimental data[14]. In fact, immunohistochemistry of *Salmonella* and MPO in infected mouse spleen
58 showed that most MPO bound to *Salmonella* (Fig. 1e), suggesting precise targeting of HOCl
59 generation and its damaging action to the pathogen surface.

60 At normal MPO concentrations around 1 mM in the phagosome[8], the model predicted efficient
61 conversion of O_2^- to HOCl (80% of the optimal theoretical yield of ½ HOCl per O_2^-; Fig. 1a, right;
62 Fig. 1.b) consistent with previous experimental[1] and modeling results[8]. HOCl (and its reaction
63 products such as chloramines[14]) are likely the main bactericidal ROS under these conditions, since
64 efficient scavenging of O_2^- and H_2O_2 by MPO would limit the concentrations of these other ROS to
65 levels (17.4 μM, 1.2 μM) that *Salmonella* could easily detoxify with its peroxidases and catalase
66 (internal H_2O_2 concentration, 0.77 μM; well below the toxicity threshold of about 2 μM[11]; Fig. 1 d).
67 Due to its low phagosomal concentration, H_2O_2 would leak only slowly from the phagosome under
68 these conditions (Fig. 1b).

69 These data suggested that absence/presence of MPO alters the bactericidal ROS (H_2O_2 vs.
70 HOCl), but has little impact on overall *Salmonella* killing. Our results differ somewhat from previous
71 interpretations of computational modeling results that suggested O_2^-, but not H_2O_2, as the most
72 important bactericidal ROS when MPO activity is low[8]. However, *Salmonella* and other pathogens
73 have potent superoxide dismutases[15] that detoxify O_2^- at very high, diffusion-limited rates[16,17],
74 whereas H_2O_2 in *Salmonella* compartments easily reach micromolar concentrations despite their
75 catalases and peroxidases. This is sufficient for lethal damage[11], despite the observation that in vitro
76 killing with bolus injections into bacterial cultures require millimolar H_2O_2 concentrations. Under such
77 non-physiological conditions, quick consumption of reduced free iron as Fenton reaction catalyst and
78 blocking of metabolism render bacteria less vulnerable to oxidative damage[18].

79 Consistent with previous data[8], the model predicted a major role of MPO in the control of
80 ROS leakage from the phagosome (Fig. 1a, b). This was the consequence of differences in reactivity
81 and reach between the MPO substrate H_2O_2 (comparatively stable, rapid diffusion through
82 membranes)[19] and the MPO product HOCl (highly reactive, reach in the nanometer range). At normal
83 MPO, most H_2O_2 was rapidly consumed minimizing its leakage (Fig. 1a, right; Fig. 1b), but already at

partial MPO deficiency (13% of normal), H_2O_2 leakage would reach rates above 1 million H_2O_2 molecules s^{-1}, surpassing HOCl production (Fig. 1b). A major role of MPO might thus be the confinement of reactive oxygen species and their damaging actions to the neutrophil phagosome during oxidative bursts.

MPO controls H_2O_2 leakage from *Salmonella*-stimulated human neutrophils in vitro

H_2O_2 leaking from the phagosome can be scavenged by several detoxification systems in the neutrophil cytosol[20]. However, a substantial fraction of H_2O_2 would still escape from the phagosome through the cytosol to the extracellular space[19]. Early experimental data suggested little H_2O_2 release in the first few minutes after microbial stimulation of neutrophils, with weak impact of MPO[21,22]. We revisited this issue with purified human neutrophils in vitro using longer observation times. Stimulation with heat-killed *Salmonella* resulted in typical neutrophil oxygen consumption kinetics and luminol chemoluminescence (a specific read-out for MPO activity[23]) with peaks at 20 to 40 min. (Fig. 2a, left, middle). An assay using horseradish peroxidase and Amplex Red that reports H_2O_2 in the extracellular medium, indicated significant H_2O_2 leakage from neutrophils throughout the entire oxidative burst (Fig. 2a, right).

To modulate MPO activity, we used the specific inhibitor ABAH[24]. MPO inhibition in intact human neutrophils required rather high ABAH concentrations (IC_{50} about 200 μM under our assay conditions) compared to much lower inhibitory concentrations (IC_{50} = 3 μM) for neutrophil lysates (Supplementary Fig. 1a). About 60-fold higher IC_{50} values for MPO in intact cells vs. freely accessible MPO were consistent with previous reports[23,24], and might reflect low saturation of MPO with endogenously generated H_2O_2 in phagosomes and/or poor intracellular drug penetration. At such high concentrations, ABAH reduced MPO activity and enhanced extracellular H_2O_2 leakage during stimulation with live or heat-killed *Salmonella* (Fig. 2c), or the fungal pathogen *Candida albicans* (Supplementary Fig. 1c). These data were consistent with the computational predictions of enhanced H_2O_2 leakage at low MPO activities. Another reagent to detect MPO activity, and more selectively

HOCl production[25], 3′-(p-aminophenyl) fluorescein (APF), gave similar results (Supplementary Fig. 1b). The release of H_2O_2 did not correlate with differential oxygen consumption (Fig. 2d, Supplementary Fig. 1d,e). Inhibiting NADPH oxidase with DPI largely abolished luminol/APF oxidation, extracellular H_2O_2 leakage, and oxygen consumption (Fig. 2c; Supplementary Fig. 1b, 1e), as expected. ABAH and DPI did not affect neutrophil degranulation as measured by three different assays[26] (Supplementary Fig. 1f). Both inhibitors did not cause detectable toxicity under our conditions (Supplementary Fig. 1g).

We next tested neutrophils from donors with partial or severe MPO deficiency according to standard clinical cytometry (Fig. 2b). As expected, MPO-deficient neutrophils had lower MPO activities compared to normal donors, and this was associated with strongly increased H_2O_2 release (Fig. 2c; Supplementary Fig. 1c). MPO activity and extracellular H_2O_2 leakage had a highly significant inverse relationship (Fig. 2e), consistent with our model predictions. Similarly, the cytometry parameter for MPO, the "mean peroxidase index (MPXI)", correlated with MPO activity but had a significant inverse correlation with H_2O_2 release (Supplementary Fig. 1h). These data demonstrated that neutrophils release H_2O_2 depending on their MPO activity.

In most experiments, we used particulate pathogen material (*Salmonella, Candida*) that trigger oxidative bursts at the phagosome membrane[27]. For comparison, we also stimulated neutrophils with phorbol esters (PMA) that induce oxidative bursts predominantly at the cell surface[27]. Under these conditions, partial blocking of MPO did not significantly alter H_2O_2 release (Supplementary Fig. 1i). Diffusion of reactants at the cell surface and altered activities of NADPH oxidase and the various MPO enzymatic reactions (both consuming and generating H_2O_2)[8] might result in a balanced MPO-mediated H_2O_2-production and –consumption under these somewhat artificial conditions. Future work might clarify this issue.

MPO controls H_2O_2 release and tissue damage in *Salmonella*-infected mice

In a mouse typhoid fever model[28], neutrophils and inflammatory monocytes provide strong, yet incomplete, control of *Salmonella*[29-32] through NADPH oxidase-mediated mechanisms[9], suggesting a key importance of oxidative bursts and ROS. In humans, neutropenia is sometimes associated with *Salmonella* bacteremia although endogenous pathogens are much more frequent, whereas NADPH oxidase defects are associated with severe *Salmonella* infections[33]. In contrast to the strong impact of NADPH oxidase deficiency, *Salmonella enterica* serovar Typhimurium grows only slightly faster in MPO-deficient mice compared to congenic wild-type mice (about 3fold higher spleen loads at day 4 post-infection, a minor difference compared to the overall 1'000 to 10'000fold increase during the same time interval)[9]. To obtain equivalent *Salmonella* spleen loads at day 4 (Fig. 3a), we infected MPO-mice with a 2-3 fold lower dose in this study.

To determine extracellular H_2O_2 release in vivo, we used a H_2O_2-specific *Salmonella* biosensor[9] carrying a transcriptional fusion of the *katGp* promoter to *gfp* in addition to constitutively expressed mCherry. *katGp* is controlled by the transcription factor OxyR that is activated by direct reaction of cysteines with H_2O_2[34] in the sub-micromolar range[35]. Biosensor *Salmonella* thus show always red fluorescence (when alive), enabling their discrimination from host debris (Fig. 3b), and additional green fluorescence when exposed to H_2O_2 at levels above 0.1 μM with up to 100fold induction when optimally stimulated[9] (Fig. 3c). This *Salmonella* H_2O_2 biosensor showed more[9] and brighter GFP^{hi} cells in MPO-deficient mice compared to congenic mice (Fig. 3d, e), suggesting an increased fraction of H_2O_2-exposed *Salmonella*, as well as higher levels of exposure.

The majority of GFP^{hi}, H_2O_2-exposed *Salmonella* in MPO-deficient mice resided in $F4/80^{hi}$ resident macrophages within the red pulp (Fig. 3f, g), the major host cell type harboring live *Salmonella* in spleen[9]. This was initially surprising, as neutrophils and inflammatory monocytes generate much stronger oxidative bursts compared to macrophages[1,36]. Moreover, neutrophils and monocytes, but not macrophages, normally express MPO[37] and would thus be primarily affected by MPO deficiency. Apparently, H_2O_2 leaking from MPO-deficient neutrophils/monocytes *in vivo* diffused through the surrounding tissue to reach resident macrophages and their intracellular biosensor *Salmonella*.

Previous studies have reported similar or altered neutrophil tissue infiltration for MPO-deficient mice in various disease models[38-45] which could affect oxidative stress levels. However, in the typhoid fever model neutrophil recruitment as detected by an antibody to Ly-6G was similar in infected wild-type and MPO-deficient mice (Fig. 4c, left). MPO-deficient human individuals had also rather normal blood neutrophil counts compared to controls [$(3.2 \pm 0.5) \times 10^9$ ml^{-1} vs. $(3.4 \pm 0.3) \times 10^9$ ml^{-1}; N 5, 8; $P > 0.05$].

While less reactive compared to HOCl, H_2O_2 is still a strong oxidant that can damage a large range of biomolecules, especially when in contact with metals, nitric oxide, etc.[46]. Indeed, infected MPO deficient mice that had higher H_2O_2 tissue levels, had also strongly exacerbated lipid peroxidation in the spleen red pulp (where most *Salmonella* and neutrophils/monocytes resided) as detected by the reaction product 4-HNE[47,48] (Fig. 4a, c), and slightly, but significantly increased DNA damage based on increased levels of 8-OHdG [48] (Fig. 4b, c), compared to infected wild-type mice. These oxidative damages occurred sometimes within or close to *Salmonella* (based on co-localization with an antibody to LPS), but most damage affected host components in CD11b^{hi} cells (neutrophils and monocytes with potent oxidative bursts), as well as CD11b^{low} bystander cells (Fig. 4a, b, insets) consistent with ROS leakage and diffusion through the tissue. Uninfected mice showed background staining in the spleen white pulp, but no detectable damage in the spleen red pulp (Supplementary Figure 2). Together, these data suggested that ROS, which are generated as part of an inflammatory response to infection, are released and cause exacerbated collateral tissue damage unless MPO confines them to intracellular compartments (Fig. 4d).

Discussion

Several pathogens such as *Salmonella* have versatile stress defense mechanisms. Killing these sturdy pathogens requires aggressive immune attacks with high local intensity, but this inevitably poses a risk of excessive self-damage in host tissues. Our data show how host immunity can solve this fundamental problem for a crucial antimicrobial mechanism, the employment of reactive oxygen species (ROS). During oxidative bursts, neutrophils use NADPH oxidase to generate high fluxes of superoxide, which spontaneously dismutates to H_2O_2. The large amount of H_2O_2 that these cells generate is sufficient to kill *Salmonella*, thus achieving the primary objective - microbial target destruction. However, H_2O_2 can also readily leak to the surrounding host tissue posing a risk of substantial collateral damage. Neutrophils use the highly abundant protein MPO to solve this problem by converting stable diffusible H_2O_2 into HOCl, which rapidly reacts with biomolecules within a few nanometers. MPO directly binds to the surface of various microbes including *Salmonella* (Fig. 1e) and *Staphylococcus aureus*[1], thus enabling precision-targeting of pathogens with intense oxidative attacks, while mitigating the risk of collateral damage (Fig. 4a, b, c). Interestingly, MPO is largely absent in resident tissue macrophages that generate ROS at about 10-fold lower rates compared to neutrophils[10], resulting in a lower risk of collateral damage.

Without self-protecting MPO, host tissues experience exacerbated oxidative tissue damage such as lipid peroxidation and DNA oxidation during infection. Increased oxidative damage during infections could have cumulative consequences over the lifetime of an individual even if the consequences on organ function and survival during a single infection might be moderate. Repeated oxidative damage can contribute to multiple diseases such as neurodegenerative and cardiovascular diseases and cancer as well as accelerated aging[49,50]. Human data are scarce but early studies reported an increased cancer incidence in patients with complete MPO deficiency[51], whereas single nucleotide polymorphisms that modulate MPO activity have weak if any impact on cancer risk[52]. Indeed, our computational model and experimental data suggest that detrimental effects should appear mostly in patients with severe/complete MPO deficiency (Fig. 1b, Fig. 2c), which is rare (in contrast to partial deficiency[1]). Importantly, studies have only been carried out in industrialized countries where human

209 infections have become greatly reduced in modern times[53], reducing the lifetime impact of
210 inflammation, collateral damage, and MPO deficiency[1]. On the other hand, long-term treatment with
211 MPO inhibitors could exacerbate these issues, and this should perhaps be considered during the
212 current clinical development of such drugs.

213 Our results differ from a study of zymosan-induced peritonitis showing that MPO actually
214 promotes lipid peroxidation[54]. Zymosan-induced peritonitis causes extensive cell death of neutrophils
215 within a few hours[55], and released MPO can then access and broadly damage extracellular host
216 molecules. Extracellular MPO release might be also involved in other disease models in which MPO
217 causes exacerbated immune pathology[1,40,42]. In contrast, detectable host cell death is rare in our mouse
218 typhoid fever model (around 1% of all infected cells)[56], thus preserving intracellular containment of
219 MPO and its damaging action.

220 Myeloperoxidase generates highly bactericidal agents that contribute to control of pathogens
221 such as *Staphylococcus aureus*[1] and *Candida*[57], and can trigger NET formation. This study shows that
222 MPO has an additional major function in mitigating collateral tissue damage during oxidative
223 antimicrobial attacks, by converting diffusible long-lived H_2O_2 that can leak out and cause damage in
224 the surrounding tissue, into highly reactive, microbiocidal, and locally confined HOCl at the pathogen
225 surface (Fig. 4e). More work will be required to fully assess the impact of this protective mechanism
226 in humans.

227

Methods

Modeling of oxidative bursts in neutrophil phagosomes

We built a diffusion-reaction model based on a previous neutrophil phagosome model[8] and our previous model of *Salmonella* oxidative stress defense[9], which are both based on experimentally determined parameters (see Supplementary Note). The model covers O_2^- generation by NADPH oxidase; O_2^- protonation equilibrium; spontaneous O_2^- dismutation; reactions of O_2^- catalyzed by myeloperoxidase or *Salmonella* superoxide dismutases SodA, SodB, SodCI; reactions of H_2O_2 catalyzed by myeloperoxidase or *Salmonella* catalase KatG or peroxidases AhpC, Tsa, Tpx; generation of HOCl by reaction of MPO compound I with chloride and MPO side reactions; and diffusion of HO_2 and H_2O_2 across the phagosomal membrane as well as *Salmonella* outer and inner membranes. Simulations using the Simulink feature of MATLAB were run until steady state concentrations were reached. Code is available upon request from the corresponding author.

MPO-deficient human individuals and normal volunteers

The study was approved by the responsible Ethics Committee (EKNZ 2015-187) and in compliance with the Declaration of Helsinki. Study participants signed an informed consent form.
Fresh venous blood was drawn in 2.7 ml polyethylene tubes containing 1.6mg EDTA/ml blood (Sarsted) and analyzed within two hours on full-automated Advia 2120 hematological analyzer (Bayer) at Hematology Routine Diagnostics Laboratory, University Hospital Basel. MPO level was determined from a Perox diagram according to cell size and peroxidase activity. MPO Index (MPXI) was calculated according to the formula: MPXI=121.1-2.38 x A(degrees), where A(degrees) describes the angle through the center of the deficient cluster and the baseline of the diagram[58].

Human PMN isolation

Human PMN were isolated as previously described[59]. In brief, human peripheral blood was collected in 7.5 ml polyethylene tubes containing 1.6 mg EDTA/ml blood (Sarsted), mixed with 3% Dextran (Pharmacia) / NaCl solution supplemented with 10 ug/ml Polymyxin-B (Calbiochem) in a ratio of 2:1. Erythrocyte sedimentation occurred after incubation for 30 min at 37°C in a 5% CO_2 incubator. Then

the leukocyte-rich plasma was aspirated and centrifuged for 7 min at 1400 rpm, 4°C. The pellet was resuspended and transferred to a discontinuous Percoll gradient with 53% and 67% Percoll (GE Healthcare). Percoll Gradient centrifugation was performed for 30 min at 1400 rpm, 4°C, no braking. The visible ring containing PMN fraction was collected and washed in 0.9% NaCl, resuspended in RPMI (Invitrogen Gibco) + 10% FBS and counted with Türk solution and an automatic cell counter system ADAM (Digital Bio). Purity and viability was routinely >97% and >99%, respectively. If necessary, hypotonic erythrocyte lysis was performed with erythrocyte lysis buffer (Biolegend). Neutrophils were distributed and incubated for 15 min before stimulation.

Pathogen cultures

Salmonella strains used in this study were derived from *Salmonella enterica* serovar Typhimurium *SL1344 hisG rpsL xyl*[60,61]. The H_2O_2 biosensor construct p*katGp-gfpOVA* was described previously[9]. *Salmonella* were cultured at 37°C with aeration (200 rpm) in Lennox LB with addition of 90 μg ml^{-1} streptomycin with or without 100 μg ml^{-1} ampicillin. For in vitro experiments, stationary phase *Salmonella* were opsonized in 10% human serum in PBS for 20min at 37°C, washed with PBS, and diluted to a multiplicity of infection (MOI) of 30 for immediate use (live *Salmonella*). Alternatively, *Salmonella* were grown to mid-log phase, washed twice in PBS and heat-inactivated at 99°C for 15 min. Heat-inactivated *Salmonella* were opsonized in 10% human serum in PBS for 20 min at 37°C, washed with PBS, and diluted to MOI 200 for immediate use (heat-inactivated *Salmonella*).

Candida albicans SC5314 was grown overnight in yeast peptone dextrose (YPD, BD Difco) media at 37°C. A subculture was inoculated 1:100 and grown to mid-log phase. *C. albicans* was washed twice with 0.9% NaCl and heat-inactivated at 95°C for 1 h. *C. albicans* was opsonized in 10% human serum in PBS for 20 min at 37°C, washed with PBS and diluted to MOI 1 for immediate use.

MPO acitivity assays

MPO activity of PMN was measured using luminol-enhanced chemoluminescence or 3′-(p-aminophenyl) fluorescein (APF) fluorescence. In brief, $2x10^5$ cells were incubated in RPMI+10% FCS for 1h at 37°C, 5% CO_2 without inhibitors, or with 500 μM ABAH or 10 μM DPI. Neutrophils were

stimulated with opsonized *Salmonella*, *Candida albicans*, or 1 nM PMA in the presence of 10% human serum and 100 µM luminol (Fluka) in HBSS (Invitrogen, Gibco) containing 0.1% glucose (Braun). Chemiluminescence was measured at 5 min intervals at 37°C with a luminometer (Microlumat Plus, Berthold Technologies). APF fluorescence was measured with flow cytometry. Values were corrected based on unstimulated controls and initial time points.

Hydrogen peroxide release of human neutrophils

Extracellular H_2O_2 release was measured by the production of Resofurin from Amplex Red (Invitrogen). In brief, $1x10^5$ cells/well were treated with or without inhibitors in RPMI containing 10% FCS for 1h at 37°C, 5% CO_2. Cells were washed once and incubated in 50µM Amplex Red + 0.1U/mL horse radish peroxidase (HRP, Sigma) in KRPG buffer (145 mM NaCl, 5.7 mM sodium phosphate, 4.86 mM KCl, 0.54 mM $CaCl_2$, 1.22 mM $MgSO_4$, 5.5 mM glucose, pH 7.35). Neutrophils were stimulated with *Salmonella* or *Candida albicans* and fluorescence was measured at 5 min intervals at 37°C with a fluorescence plate reader (490 nm excitation, 590 nm emission). Values were corrected based on negative controls without HRP and initial time points. H_2O_2 concentration was determined using standard curves obtained with defined H_2O_2 concentrations.

Oxygen Consumption Rate

Oxygen Consumption Rate was measured with a Seahorse XF-96 metabolic extracellular flux analyzer (Seahorse Bioscience). Human peripheral blood derived neutrophils pretreated or not with inhibitors were resuspended in KRPG buffer and plated onto Seahorse cell plates (3×10^5 cells per well) coated with Cell-Tak (BD Bioscience). Heat-killed *C. albicans* SC5314 (MOI=2) or heat-killed *Salmonella* Typhimurium SL1344 (MOI=200) was directly applied onto plated cells via the instrument's injection port. The experimental parameters were set at 3 min mixture / 0 minutes wait / 3 min measurement for 23 cycles.

Peroxidation activity of MPO in intact and lysed neutrophils

Peroxidation activity was quantified by the production of Resofurin from Amplex Red. To determine MPO activity of neutrophil lysates $1x10^5$ cells/well were lysed with 1x lysis buffer (Cell signaling, No. 9803) and treated with increasing ABAH concentrations (0 μM to 500 μM) in RPMI+10% FCS. 50 μM Amplex Red + 5 μM H_2O_2 were added and fluorescence was measured after 30 min incubation at 37°C. To determine MPO activity of intact neutrophils $1x10^5$cells/well were washed 3 x with PBS after 1h treatment of increasing ABAH concentrations (0 μM to 500 μM) in RPMI+10% FCS, and then lysed. 50 μM Amplex Red + 5 μM H_2O_2 were added and fluorescence was measured after 30 min incubation at 37°C. MPO activity was determined using standard curves obtained with defined MPO (Sigma M6908) concentrations.

Neutrophil degranulation

MPO release in neutrophil supernatants at 75 min after stimulation was quantified with the Human MPO DuoSet ELISA kit (R&D, No. DY3174) using a MPO standard for calibration following the manufacturer's instructions. Optical density of standards and neutrophil supernatants was determined in triplicates at 450 nm using an ELISA microplate reader (Biotek, Synergy H3).

Appearance of CD63 and CD66 at the neutrophil surface following 75 min stimulation was quantified with flow cytometry. Cells were incubated for 15 min at room temperature with human TruStain FcX™ Blocking solution (Biolegend, No. 422302, 2μl/test), followed by incubation with FITC anti-human CD66b (Biolegend, Clone G10F5, No. 305104) and APC anti-human CD63 (Biolegend, Clone H5C6, No. 353008) for 30 minutes at 4°C. Samples were analyzed using a BD Accuri C6 flow cytometer using FL-1 (488nm laser, 530/30 filter) and FL-4 (640nm laser, 675/25 filter) channels.

Mouse Infections and Tissue Collection

All animal experiments were approved (license 2239, Kantonales Veterinäramt Basel) and performed according to local guidelines (Tierschutz-Verordnung, Basel) and the Swiss animal protection law (Tierschutz-Gesetz). Female 8-10 weeks old B6.129X1-MPO$^{tm1Lus/J}$ as well as age- and sex-matched C57BL/6J congenic mice, were infected by tail vein injection of 800-2800 *Salmonella* in 100 μl PBS

and euthanized at 4 days post infection. Spleen tissue was collected from each mouse and dissected into several pieces. CFU counts were determined by plating. We estimated sample size by a sequential statistical design. We first infected 4 mice each based on effect sizes and variation observed in our previous study[9]. Biosensor responses and oxidative tissue damage analysis suggested that 4 additional mice in each group would be sufficient to determine statistical significance with sufficient power. This was indeed the case (see text). We did neither randomize nor blind the experiments. However, image analysis of stained section was carried out using an automated unbiased approach (see Image Analysis section).

Immunohistochemistry

2-3mm thick spleen sections were fixed with fresh 4% paraformaldehyde at 4°C for 4 h, followed by incubating in increasing sucrose concentrations from 10%-40% at 4°C. After overnight incubation in 40% sucrose, tissue was rapidly frozen in embedding media (Tissue-Tek® O.C.T; Sakura), left overnight at -80°C, and then stored at -20°C. Unfixed tissue was immediately frozen in embedding media, left overnight at -80°C, and then stored at -20°C. 10-14 µm thick cryosections were cut, put on coated glass cover slips (Thermo Scientific) and dried in a desiccator. After blocking with 1% blocking reagent (Invitrogen) and 2% mouse serum (Invitrogen) in PBST (0.05% Tween in 1X PBS pH7.4), sections were stained with primary antibodies (rat anti-CD11b, BD clone M1/70; goat anti-CSA1, KPL 01-91-99-MG, goat anti-4-HNE, Alpha Diagnostics HNE12-S, rabbit anti-myeloperoxidase, abcam 9535, goat anti-8 Hydroxyguanosine abcam 10802; rat F4/80, Serotec clone CI:A31; rat Ly-6G, BD clone 1A8). A variety of secondary antibodies were used depending on the application (Molecular probes; Cat. A-21443; S11225, S21374; A-21206; A11096, D20698, Invitrogen A31556, Santa CruzBT sc-362245). For 4-HNE and 8-Hydroxyguanosine (8-OHdG) stainings, we used unfixed sections and a horseradish peroxidase kit (Molecular probes; Cat: T-20936) to amplify the signal. Sections were mounted in fluorescence mounting medium (Dako or Vectashield), and examined with a Zeiss LSM 700 confocal microscope using glycerol 25X, 40X, and 63X objectives. Tiles covering an entire spleen section were stitched together. High resolution images were obtained with a Zeiss LSM 800 using Airy Scanning.

Image Analysis

For quantitative analysis of lipid peroxidation and DNA damage on antibody-stained spleen sections, we used an unbiased, automated protocol in the bioimage informatics platform icy[62]. This protocol was established to minimize the impact of differences in staining intensities between individual samples. Each image consisted of 3 channels (DAPI, nuclei; 4-HNE, lipid peroxidation or 8-OHdG, DNA damage; CD11b, infiltrating neutrophils and monocytes). In a first step, the whole tissue area was segmented using the combined intensities from all three channels. In a next step a threshold was applied to create a segmentation of red pulp containing $CD11b^{hi}$ cells. The threshold value was set using Huang's method, which minimizes fuzziness[63] to avoid over-segmentation of noisy regions, especially at segmentation borders. Next the $CD11b^{hi}$ area was subtracted from the whole tissue area to create a segmentation of white pulp with little CD11b staining. For detecting the proportion of 4-HNE^{hi} (or 8-$OHdG^{hi}$) pixels in the $CD11b^{hi}$ and $CD11b^{lo}$ regions, we used as threshold the sum of the mean 4-HNE signal over the entire tissue section + 3 times the standard deviation. The staining index was then determined as the ratio of 4-HNE^{hi} pixels proportions in $CD11b^{hi}$ over $CD11b^{lo}$ regions. As a much simpler alternative, we also used a simple threshold of 100 across all samples, which gave similar results.

Flow Cytometry

Spleen homogenates were prepared for flow cytometry as described [9]. Relevant spectral parameters of 10,000 to 50,000 *Salmonella* were recorded in a FACS Fortessa II equipped with 488 nm and 561 nm lasers (Becton Dickinson), using thresholds on SSC and FSC to exclude electronic noise (channels: GFP, excitation 488 nm, emission 502-525; mCherry, excitation 561 nm, emission 604-628 nm; yellow autofluorescence channel, excitation 488 nm, emission 573-613 nm; infrared autofluorescence channel, excitation 561 nm, emission 750-810 nm). Data processing was done with FlowJo and FCS Express.

Data availability

The data that support the findings of this study are available from the corresponding author upon request.

Correspondence and requests for materials should be addressed to D.B.

Acknowledgements

We thank K. Ullrich and R. Kühl for taking blood from human donors and all donors for blood donations. We thank I. Bartholomaeus and A. Martin for support with confocal microscopy. This study was supported in part by grants from Swiss National Foundation (310030_156818 to D.B., PZ00P3_142403 to N.K., and PP00P3_144863 to M.R.) and Gebert Rüf Foundation (GRS 058/14 to C.H., A.-V. B and M.R.).

Author contributions

N.S., P.F., B.F., N.E., A.T.P., J.L., and D.B. performed experiments and analyzed the data; O.C. and D.B. wrote code and ran the computational models; A.-V.B., C.H., and M.R. recruited patients; N.S., P.F., W.D.H., N.K., and D.B. designed experiments; and N.S., P.F., and D.B. wrote the paper.

Additional information

Supplementary information is available online. Reprints and permissions information is available online at www.nature.com/reprints.

References

1 Klebanoff, S. J., Kettle, A. J., Rosen, H., Winterbourn, C. C. & Nauseef, W. M. Myeloperoxidase: a front-line defender against phagocytosed microorganisms. *J Leukoc Biol* **93**, 185-198, doi:10.1189/jlb.0712349 (2013).

2 Arnhold, J., Furtmuller, P. G., Regelsberger, G. & Obinger, C. Redox properties of the couple compound I/native enzyme of myeloperoxidase and eosinophil peroxidase. *European journal of biochemistry / FEBS* **268**, 5142-5148 (2001).

3 Storkey, C., Davies, M. J. & Pattison, D. I. Reevaluation of the rate constants for the reaction of hypochlorous acid (HOCl) with cysteine, methionine, and peptide derivatives using a new competition kinetic approach. *Free radical biology & medicine* **73**, 60-66, doi:10.1016/j.freeradbiomed.2014.04.024 (2014).

4 Parker, H. & Winterbourn, C. C. Reactive oxidants and myeloperoxidase and their involvement in neutrophil extracellular traps. *Front Immunol* **3**, 424, doi:10.3389/fimmu.2012.00424 (2012).

5 Metzler, K. D., Goosmann, C., Lubojemska, A., Zychlinsky, A. & Papayannopoulos, V. A myeloperoxidase-containing complex regulates neutrophil elastase release and actin dynamics during NETosis. *Cell reports* **8**, 883-896, doi:10.1016/j.celrep.2014.06.044 (2014).

6 Davies, M. J., Hawkins, C. L., Pattison, D. I. & Rees, M. D. Mammalian heme peroxidases: from molecular mechanisms to health implications. *Antioxidants & redox signaling* **10**, 1199-1234, doi:10.1089/ars.2007.1927 (2008).

7 Ruggeri, R. B. *et al.* Discovery of 2-(6-(5-Chloro-2-methoxyphenyl)-4-oxo-2-thioxo-3,4-dihydropyrimidin-1(2H)-yl)acet amide (PF-06282999): A Highly Selective Mechanism-Based Myeloperoxidase Inhibitor for the Treatment of Cardiovascular Diseases. *Journal of medicinal chemistry* **58**, 8513-8528, doi:10.1021/acs.jmedchem.5b00963 (2015).

8 Winterbourn, C. C., Hampton, M. B., Livesey, J. H. & Kettle, A. J. Modeling the reactions of superoxide and myeloperoxidase in the neutrophil phagosome: implications for microbial killing. *J Biol Chem* **281**, 39860-39869, doi:10.1074/jbc.M605898200 (2006).

9 Burton, N. A. *et al.* Disparate impact of oxidative host defenses determines the fate of Salmonella during systemic infection in mice. *Cell host & microbe* **15**, 72-83, doi:10.1016/j.chom.2013.12.006 (2014).

10 Imlay, J. A. in *EcoSal* (ed R. III.; Kaper Curtiss, J.B.; Squires, C.L.; Karp, P.D.; Neidhardt, F.C.; Slauch, J.M.) Ch. Modul 5.4.4, (ASM Press, 2009).

11 Seaver, L. C. & Imlay, J. A. Hydrogen peroxide fluxes and compartmentalization inside growing Escherichia coli. *J Bacteriol* **183**, 7182-7189 (2001).

12 Makino, N., Sasaki, K., Hashida, K. & Sakakura, Y. A metabolic model describing the H2O2 elimination by mammalian cells including H2O2 permeation through cytoplasmic and peroxisomal membranes: comparison with experimental data. *Biochimica et biophysica acta* **1673**, 149-159, doi:10.1016/j.bbagen.2004.04.011 (2004).

13 Kundrat, P., Bauer, G., Jacob, P. & Friedland, W. Mechanistic modelling suggests that the size of preneoplastic lesions is limited by intercellular induction of apoptosis in oncogenically transformed cells. *Carcinogenesis* **33**, 253-259, doi:10.1093/carcin/bgr227 (2012).

14 Green, J. N., Kettle, A. J. & Winterbourn, C. C. Protein chlorination in neutrophil phagosomes and correlation with bacterial killing. *Free radical biology & medicine* **77**, 49-56, doi:10.1016/j.freeradbiomed.2014.08.013 (2014).

15 Korshunov, S. S. & Imlay, J. A. A potential role for periplasmic superoxide dismutase in blocking the penetration of external superoxide into the cytosol of Gram-negative bacteria. *Mol Microbiol* **43**, 95-106 (2002).

16 Stroppolo, M. E. *et al.* Single mutation at the intersubunit interface confers extra efficiency to Cu,Zn superoxide dismutase. *FEBS Lett* **483**, 17-20 (2000).

17 Bull, C. & Fee, J. A. Steady-state kinetic studies of superoxide dismutases: properties of the iron containing protein from Escherichia coli. *Journal of the American Chemical Society* **107**, 3295-3304, doi:10.1021/ja00297a040 (1985).

18 Park, S., You, X. & Imlay, J. A. Substantial DNA damage from submicromolar intracellular hydrogen peroxide detected in Hpx- mutants of Escherichia coli. *Proc Natl Acad Sci U S A* **102**, 9317-9322 (2005).

19 Winterbourn, C. C. Reconciling the chemistry and biology of reactive oxygen species. *Nature chemical biology* **4**, 278-286, doi:10.1038/nchembio.85 (2008).

20 Benfeitas, R., Selvaggio, G., Antunes, F., Coelho, P. M. & Salvador, A. Hydrogen peroxide metabolism and sensing in human erythrocytes: a validated kinetic model and reappraisal of the role of peroxiredoxin II. *Free radical biology & medicine* **74**, 35-49, doi:10.1016/j.freeradbiomed.2014.06.007 (2014).

21 Nauseef, W. M., Metcalf, J. A. & Root, R. K. Role of myeloperoxidase in the respiratory burst of human neutrophils. *Blood* **61**, 483-492 (1983).

22 Gerber, C. E., Kuci, S., Zipfel, M., Niethammer, D. & Bruchelt, G. Phagocytic activity and oxidative burst of granulocytes in persons with myeloperoxidase deficiency. *Eur J Clin Chem Clin Biochem* **34**, 901-908 (1996).

23 Gross, S. *et al.* Bioluminescence imaging of myeloperoxidase activity in vivo. *Nat Med* **15**, 455-461, doi:10.1038/nm.1886 (2009).

24 Kettle, A. J., Gedye, C. A., Hampton, M. B. & Winterbourn, C. C. Inhibition of myeloperoxidase by benzoic acid hydrazides. *Biochem J* **308 (Pt 2)**, 559-563 (1995).

25 Flemmig, J., Remmler, J., Zschaler, J. & Arnhold, J. Detection of the halogenating activity of heme peroxidases in leukocytes by aminophenyl fluorescein. *Free radical research* **49**, 768-776, doi:10.3109/10715762.2014.999676 (2015).

26 Naegelen, I. *et al.* An essential role of syntaxin 3 protein for granule exocytosis and secretion of IL-1alpha, IL-1beta, IL-12b, and CCL4 from differentiated HL-60 cells. *J Leukoc Biol* **97**, 557-571, doi:10.1189/jlb.3A0514-254RR (2015).

27 Winterbourn, C. C., Kettle, A. J. & Hampton, M. B. Reactive Oxygen Species and Neutrophil Function. *Annual review of biochemistry* **85**, 765-792, doi:10.1146/annurev-biochem-060815-014442 (2016).

28 Tsolis, R. M., Xavier, M. N., Santos, R. L. & Baumler, A. J. How to become a top model: The impact of animal experimentation on human Salmonella disease research. *Infect Immun* **79**, 1806-1814 (2011).

29 Conlan, J. W. Critical roles of neutrophils in host defense against experimental systemic infections of mice by Listeria monocytogenes, Salmonella typhimurium, and Yersinia enterocolitica. *Infect Immun* **65**, 630-635 (1997).

30 Vassiloyanakopoulos, A. P., Okamoto, S. & Fierer, J. The crucial role of polymorphonuclear leukocytes in resistance to Salmonella dublin infections in genetically susceptible and resistant mice. *Proc Natl Acad Sci U S A* **95**, 7676-7681 (1998).

31 Cheminay, C., Chakravortty, D. & Hensel, M. Role of neutrophils in murine salmonellosis. *Infect.Immun.* **72**, 468-477 (2004).

32 Dejager, L., Pinheiro, I., Bogaert, P., Huys, L. & Libert, C. Role for neutrophils in host immune responses and genetic factors that modulate resistance to Salmonella enterica serovar typhimurium in the inbred mouse strain SPRET/Ei. *Infect Immun* **78**, 3848-3860, doi:10.1128/IAI.00044-10 (2010).

33 Mastroeni, P. *et al.* Resistance and susceptibility to Salmonella infections: lessons from mice and patients with immunodeficiencies. *Reviews in Medical Microbiology* **14**, 53-62 (2003).

34 Lee, C. *et al.* Redox regulation of OxyR requires specific disulfide bond formation involving a rapid kinetic reaction path. *Nat Struct Mol Biol* **11**, 1179-1185, doi:10.1038/nsmb856 (2004).

35 Aslund, F., Zheng, M., Beckwith, J. & Storz, G. Regulation of the OxyR transcription factor by hydrogen peroxide and the cellular thiol-disulfide status. *Proceedings of the National Academy of Sciences of the United States of America* **96**, 6161-6165 (1999).

36 Swirski, F. K. *et al.* Myeloperoxidase-rich Ly-6C+ myeloid cells infiltrate allografts and contribute to an imaging signature of organ rejection in mice. *J Clin Invest* **120**, 2627-2634, doi:10.1172/JCI42304 (2010).

37 Swirski, F. K. *et al.* Myeloperoxidase-rich Ly-6C+ myeloid cells infiltrate allografts and contribute to an imaging signature of organ rejection in mice. *J Clin Invest* **120**, 2627-2634 (2010).

38 Kremserova, S. *et al.* Lung Neutrophilia in Myeloperoxidase Deficient Mice during the Course of Acute Pulmonary Inflammation. *Oxidative medicine and cellular longevity* **2016**, 5219056, doi:10.1155/2016/5219056 (2016).

39 Endo, D., Saito, T., Umeki, Y., Suzuki, K. & Aratani, Y. Myeloperoxidase negatively regulates the expression of proinflammatory cytokines and chemokines by zymosan-induced mouse neutrophils. *Inflammation research : official journal of the European Histamine Research Society ... [et al.]* **65**, 151-159, doi:10.1007/s00011-015-0899-5 (2016).

40 Brovkovych, V. *et al.* Augmented inducible nitric oxide synthase expression and increased NO production reduce sepsis-induced lung injury and mortality in myeloperoxidase-null mice. *American journal of physiology. Lung cellular and molecular physiology* **295**, L96-103, doi:10.1152/ajplung.00450.2007 (2008).

41 Homme, M., Tateno, N., Miura, N., Ohno, N. & Aratani, Y. Myeloperoxidase deficiency in mice exacerbates lung inflammation induced by nonviable Candida albicans. *Inflammation research : official journal of the European Histamine Research Society ... [et al.]* **62**, 981-990, doi:10.1007/s00011-013-0656-6 (2013).

42 Sugamata, R. *et al.* Contribution of neutrophil-derived myeloperoxidase in the early phase of fulminant acute respiratory distress syndrome induced by influenza virus infection. *Microbiology and immunology* **56**, 171-182, doi:10.1111/j.1348-0421.2011.00424.x (2012).

43 Takeuchi, K. *et al.* Severe neutrophil-mediated lung inflammation in myeloperoxidase-deficient mice exposed to zymosan. *Inflammation research : official journal of the European Histamine Research Society ... [et al.]* **61**, 197-205, doi:10.1007/s00011-011-0401-y (2012).

44 Brennan, M. L. *et al.* A tale of two controversies: defining both the role of peroxidases in nitrotyrosine formation in vivo using eosinophil peroxidase and myeloperoxidase-deficient mice, and the nature of peroxidase-generated reactive nitrogen species. *J Biol Chem* **277**, 17415-17427, doi:10.1074/jbc.M112400200 (2002).

45 Klinke, A. *et al.* Myeloperoxidase attracts neutrophils by physical forces. *Blood* **117**, 1350-1358, doi:10.1182/blood-2010-05-284513 (2011).

46 Imlay, J. A. The molecular mechanisms and physiological consequences of oxidative stress: lessons from a model bacterium. *Nat Rev Microbiol* **11**, 443-454, doi:10.1038/nrmicro3032 (2013).

47 Liou, G. Y. & Storz, P. Detecting reactive oxygen species by immunohistochemistry. *Methods Mol Biol* **1292**, 97-104, doi:10.1007/978-1-4939-2522-3_7 (2015).

48 Seki, S. *et al.* In situ detection of lipid peroxidation and oxidative DNA damage in non-alcoholic fatty liver diseases. *J Hepatol* **37**, 56-62 (2002).

49 Loft, S. & Poulsen, H. E. Cancer risk and oxidative DNA damage in man. *J Mol Med (Berl)* **74**, 297-312 (1996).

50 Finkel, T. & Holbrook, N. J. Oxidants, oxidative stress and the biology of ageing. *Nature* **408**, 239-247, doi:10.1038/35041687 (2000).

51 Lanza, F. Clinical manifestation of myeloperoxidase deficiency. *J Mol Med (Berl)* **76**, 676-681 (1998).

52 Yuzhalin, A. E. & Kutikhin, A. G. Common genetic variants in the myeloperoxidase and paraoxonase genes and the related cancer risk: a review. *Journal of environmental science and health. Part C, Environmental carcinogenesis & ecotoxicology reviews* **30**, 287-322, doi:10.1080/10590501.2012.731957 (2012).

53 Crimmins, E. M. & Finch, C. E. Infection, inflammation, height, and longevity. *Proc Natl Acad Sci U S A* **103**, 498-503, doi:10.1073/pnas.0501470103 (2006).

54 Zhang, R. *et al.* Myeloperoxidase functions as a major enzymatic catalyst for initiation of lipid peroxidation at sites of inflammation. *The Journal of biological chemistry* **277**, 46116-46122, doi:10.1074/jbc.M209124200 (2002).
55 Kolaczkowska, E., Koziol, A., Plytycz, B. & Arnold, B. Inflammatory macrophages, and not only neutrophils, die by apoptosis during acute peritonitis. *Immunobiology* **215**, 492-504, doi:10.1016/j.imbio.2009.07.001 (2010).
56 Grant, A. J. *et al.* Caspase-3-dependent phagocyte death during systemic Salmonella enterica serovar Typhimurium infection of mice. *Immunology* **125**, 28-37, doi:10.1111/j.1365-2567.2008.02814.x (2008).
57 Branzk, N. *et al.* Neutrophils sense microbe size and selectively release neutrophil extracellular traps in response to large pathogens. *Nature immunology* **15**, 1017-1025, doi:10.1038/ni.2987 (2014).
58 Kutter, D. *et al.* Consequences of total and subtotal myeloperoxidase deficiency: risk or benefit ? *Acta Haematol* **104**, 10-15, doi:41062 (2000).
59 Hjorth, R., Jonsson, A. K. & Vretblad, P. A rapid method for purification of human granulocytes using percoll. A comparison with dextran sedimentation. *Journal of Immunological Methods* **43**, 95-101 (1981).
60 Hoiseth, S. K. & Stocker, B. A. Aromatic-dependent Salmonella typhimurium are non-virulent and effective as live vaccines. *Nature* **291**, 238-239 (1981).
61 Kroger, C. *et al.* The transcriptional landscape and small RNAs of Salmonella enterica serovar Typhimurium. *Proc Natl Acad Sci U S A* **109**, E1277-1286 (2012).
62 de Chaumont, F. *et al.* Icy: an open bioimage informatics platform for extended reproducible research. *Nature methods* **9**, 690-696, doi:10.1038/nmeth.2075 (2012).
63 Huang, L.-K. & Wang, M.-J. J. Image thresholding by minimizing the measures of fuzziness. *Pattern recognition* **28**, 41-51 (1995).

595 **Figure legends**

596

597 **Fig. 1: Computational model of reactive oxygen species generation and leakage in neutrophil**
598 **phagosomes containing *Salmonella***.

599 **a,** Schematic representation of redox reactions and diffusion in neutrophil phagosomes containing
600 various concentrations of myeloperoxidase (MPO: Cpd, Compound; $MP3^+$, native MPO) and
601 *Salmonella* expressing detoxification enzymes (red), as predicted by computational modelling. Only
602 the most relevant reactions are shown. Thickness of arrows represents reaction rates as shown in the
603 inbox of the left panel. The star-like patterns represent lethal *Salmonella* damage caused by H_2O_2
604 (blue) or HOCl (orange). **b**, Predicted generation and leakage of HOCl and H_2O_2 as final host ROS
605 products (prior to damage reactions) as a function of MPO concentration. HOCl was predicted to
606 remain confined exclusively to the phagosome. **c**, Predicted *Salmonella* detoxification of H_2O_2 through
607 catalase (KatG) and peroxidases (AhpC, Tsa, Tpx). **d,** Impact of MPO concentration on H_2O_2
608 concentrations in the phagosome lumen and the *Salmonella* cytosol. The blue box and the dashed line
609 represent cytosolic concentrations above 2 μM that are lethal for *Salmonella*. **e**, Representative
610 micrograph of *Salmonella* in infected mouse spleen stained for MPO and common *Salmonella* antigen
611 (CSA). The lower panel shows a 3-dimensional surface rendering of the confocal stack. The scale bar
612 represents 2 μm.

613

614 **Fig. 2: Reactive oxygen species generation and leakage of human neutrophils in vitro**.

615 **a**, Kinetics of oxygen consumption, MPO activity (as measured by luminol oxidation), and
616 extracellular H_2O_2 release during *Salmonella* stimulation of neutrophils from one representative
617 normal human donor. Means and standard deviations of three technical replicates are shown. **b**,
618 Representative leukograms of donors with different levels of myeloperoxidase activities (MPXI,
619 mean peroxidase index). For each donor one leukogram was recorded. The red circles contain the
620 granulocyte populations. The dashed lines separate MPIXI ranges for severe or partial deficiency
621 and normal values. **c**, MPO activity and H_2O_2 release of neutrophils from eight different normal

622 donors (black circles), two partially deficient donors (grey), and two severely deficient donors (empty
623 circles) after 75 min. stimulation with live or heat-killed (HK) *Salmonella* in presence/absence of the
624 MPO inhibitor ABAH (AB) or the NADPH oxidase inhibitor DPI (Kruskal-Wallis multiple
625 comparisons test; *, $P< 0.05$; **, $P< 0.01$). **d**, Relationship between oxygen consumption and H_2O_2
626 release in neutrophils stimulated with heat-killed *Salmonella* for 75 min. Values for wells containing
627 100'000 neutrophils are shown. **e**, Relationship between MPO activity and H_2O_2 release after 75 min.
628 stimulation with live or heat-killed *Salmonella* (r, Spearman correlation coefficient).

629

630 **Fig. 3**: **H_2O_2 exposure of *Salmonella* in spleen of wild-type and MPO-deficient mice as revealed**
631 **by a *Salmonella* biosensor strain.**

632 **a**, *Salmonella* spleen loads in wild-type (B6) and MPO-deficient mice 4 days after infection (each dot
633 represents one mouse; t-test on log-transformed data; n.s., not significant). **b**, Detection of mCherry-
634 expressing *Salmonella* against a background of preponderant host debris in infected mouse spleen
635 homogenates using flow cytometry (laser excitation wavelength of 561 nm for the two channels
636 shown). The dotted box represents the acquisition gate for monitoring GFP expression in *Salmonella*.
637 One representative example of eight mice is shown. **c**, In vitro stimulation of GFP fluorescence after
638 30 min. incubation with various concentrations of H_2O_2 (flow cytometry histograms). Representative
639 data of one of three experiments are shown. **d**, Representative flow cytometry dot plots of *Salmonella*
640 biosensor in spleen homogenates of wild-type (B6) and MPO-deficient mice. The dotted red lines
641 represent a more stringent gate on mCherry positive *Salmonella*. The black dashed lines separate
642 positive biosensor responses (GFP^{hi}) from baseline *Salmonella* fluorescence. $mCherry^{lo}$ particles were
643 excluded during data acquisition to avoid excessively large data files. Even in MPO-deficient mice,
644 more than 95% of *Salmonella* biosensor cells were still not stimulated at saturating levels based on in
645 vitro induction dynamics (Fig. 3c). **e**, Quantification of flow cytometry data as shown in d, (MFI,
646 mean fluorescence intensity; N = 4, 4; t-test; ***, $P< 0.001$; **, $P< 0.01$). **f**, Localization of GFP^{hi}
647 biosensor *Salmonella* in $F4/80^{hi}$ macrophages in the vicinity of $CD11b^{hi}$ neutrophils/inflammatory
648 monocytes using immunohistochemistry of a spleen cryosection. Representative data for one out of

four MPO-deficient mice are shown. The scale bar represents 10 μm. **g**, Quantification of localization data as shown in (F) (means and standard deviations; N = 4, 4; t-test, $P< 0.001$).

Fig. 4: **Collateral tissue damage in absence of myeloperoxidase (MPO)**.

a, Lipid peroxidation in infected spleen as detected by an antibody to 4-hydroxynonenal (4-HNE). Spleen cross-sections from wild-type (B6) and MPO-deficient mice imaged at identical microscopy settings are shown. These images are representative for eight individuals of either genotype. The scale bar represents 500 μm. The inset shows a representative area at higher magnification from a different section that was also stained with an antibody to *Salmonella*-LPS (scale bar 10 μm). **b**, Nucleoside oxidative damage as detected by an antibody to 8-hydroxy-2'- deoxyguanosine ((OHdG). These images are representative for eight individuals of either genotype. The scale bar represents 100 μm. The inset shows a representative area at higher magnification from a different section that was also stained with an antibody to *Salmonella*-LPS (scale bar 10 μm). **c**, Quantification of Ly-6G staining (reflecting neutrophil numbers), 4-HNE staining (reflecting lipid oxidation), and OHdG staining (reflecting DNA damage) in the red pulp (where most *Salmonella* and $CD11b^{hi}$ host cells resided). Each dot represents one mouse (Mann-Whitney-U test; ***, $P< 0.001$; *, $P< 0.05$). **d**, Schematic model for the role of MPO. In MPO-deficient individuals (left), ROS generation in the neutrophil phagosome lead to high H_2O_2 (blue) accumulation which kills *Salmonella* (dotted red line) in the phagosome. However, most H_2O_2 leaks out from the phagosome and diffuses through the tissue where it causes collateral damage (light bolts) and is detected by live *Salmonella* (red). By contrast, in normal individuals (right) MPO at the *Salmonella* surface converts almost all generated ROS generated into HOCl (orange). HOCl immediately reacts with nearby biomolecules causing lethal *Salmonella* damage (large light bolt). Because of this efficient scavenging by MPO, little H_2O_2 leaks out from the phagosome resulting in minimal collateral damage under these conditions.

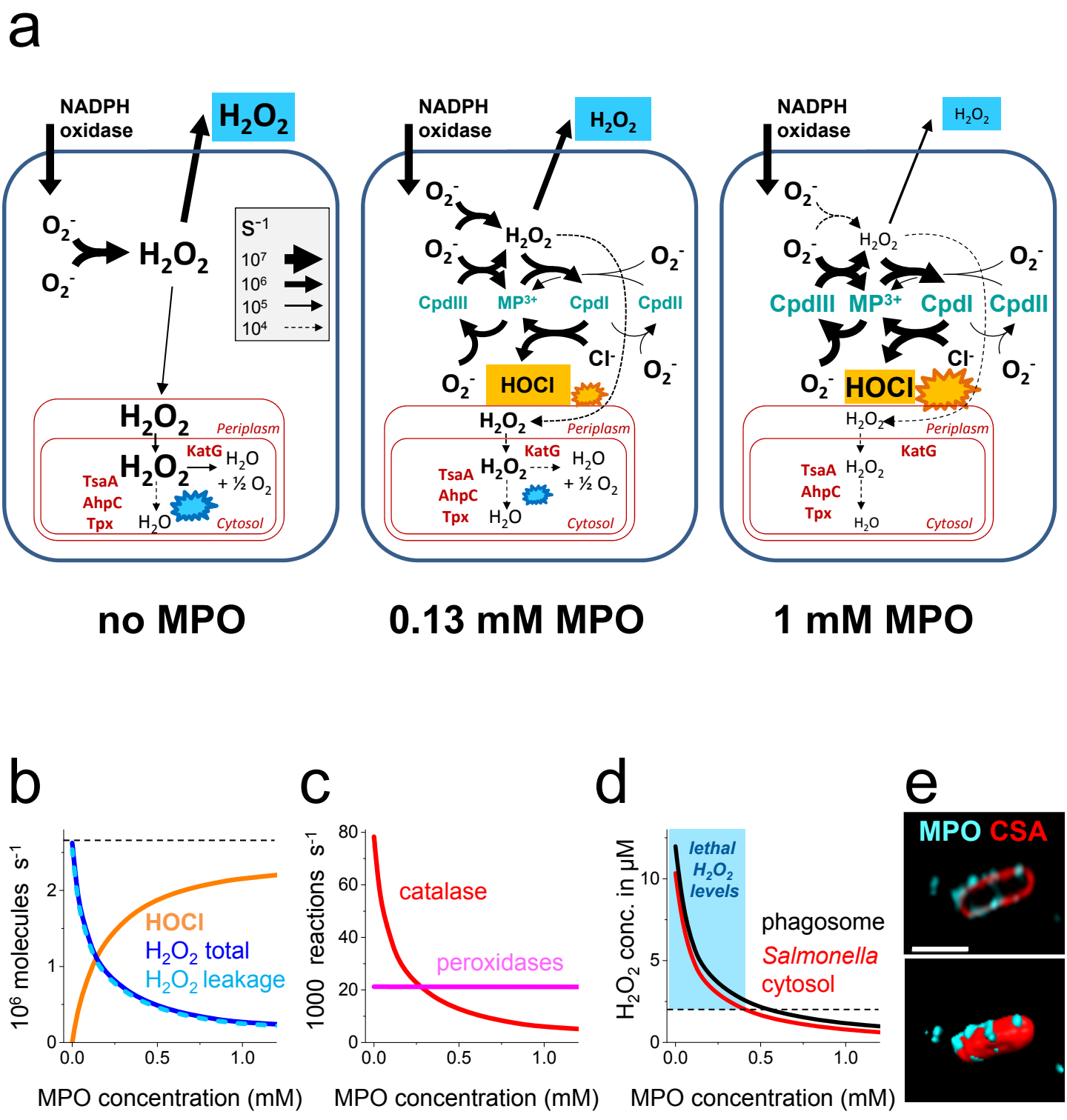
a
NADPH oxidase
H2O2
O2-
S-1
10^7
10^6
10^5
10^4
Periplasm
Cytosol
KatG
TsaA
AhpC
Tpx
H2O
+ ½ O2
CpdIII
MP3+
CpdI
CpdII
Cl-
HOCl
no MPO
0.13 mM MPO
1 mM MPO
b
10^6 molecules s-1
HOCl
H2O2 total
H2O2 leakage
MPO concentration (mM)
c
1000 reactions s-1
catalase
peroxidases
MPO concentration (mM)
d
H2O2 conc. in µM
lethal H2O2 levels
phagosome
Salmonella
cytosol
MPO concentration (mM)
e
MPO CSA

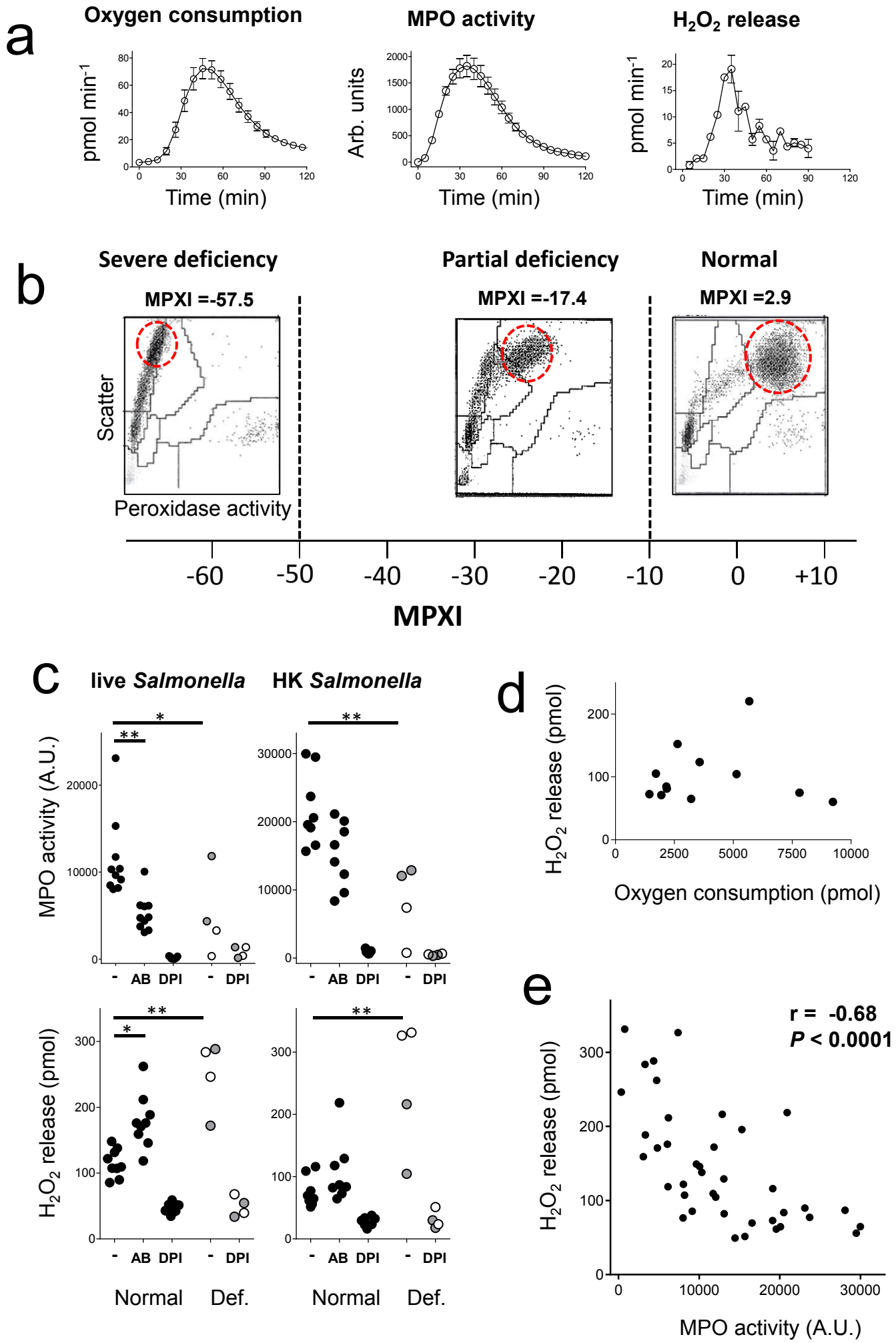
a
Oxygen consumption
MPO activity
H2O2 release
pmol min-1
Arb. units
Time (min)
b
Severe deficiency
Partial deficiency
Normal
MPXI =-57.5
MPXI =-17.4
MPXI =2.9
Scatter
Peroxidase activity
-60
-50
-40
-30
-20
-10
0
+10
MPXI
c
live Salmonella
HK Salmonella
MPO activity (A.U.)
H2O2 release (pmol)
AB
DPI
Normal
Def.
d
H2O2 release (pmol)
Oxygen consumption (pmol)
e
r = -0.68
P < 0.0001
H2O2 release (pmol)
MPO activity (A.U.)

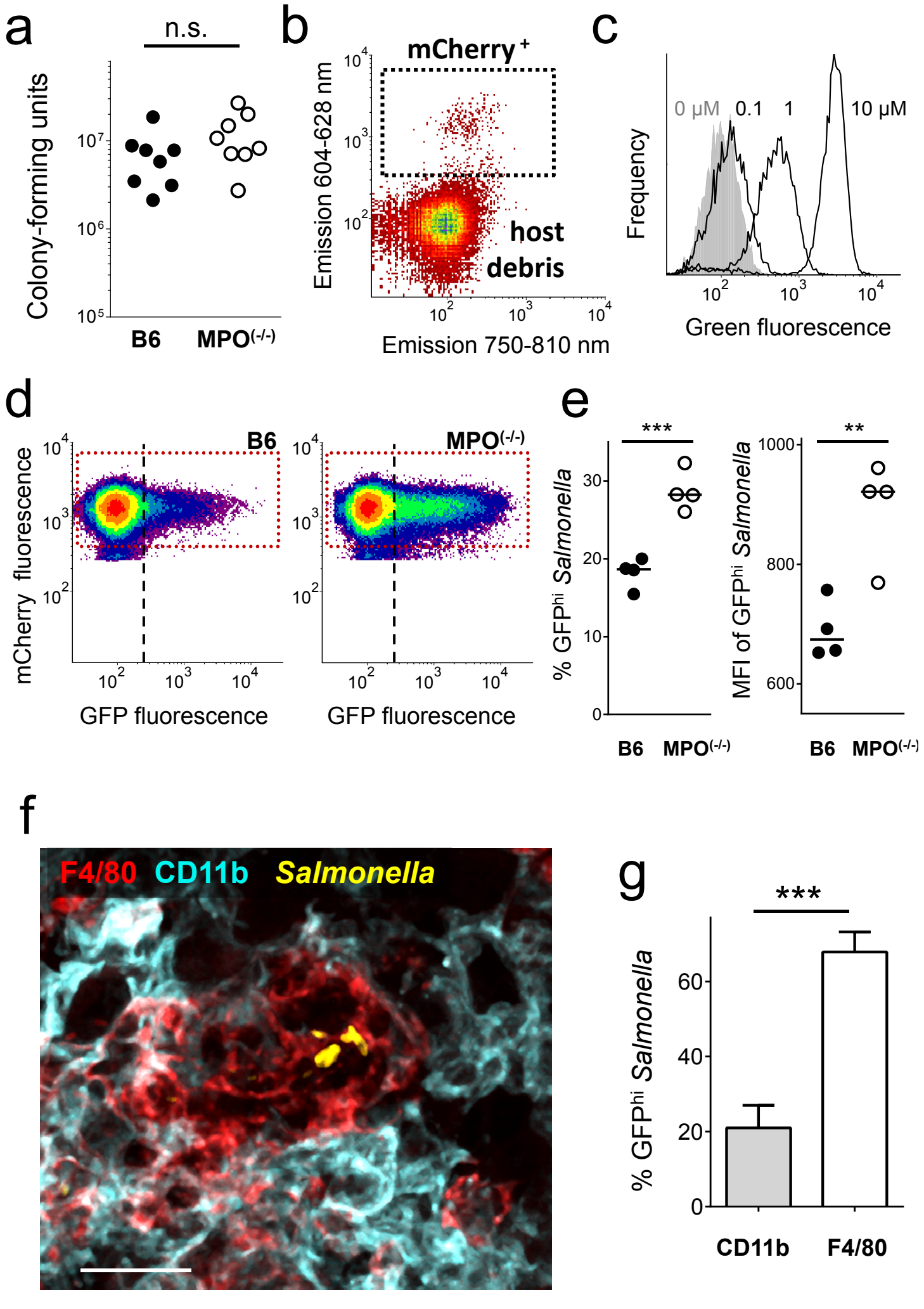
a
n.s.
Colony-forming units
B6
MPO(-/-)
b
mCherry+
host debris
Emission 604-628 nm
Emission 750-810 nm
c
0 μM
0.1
1
10 μM
Frequency
Green fluorescence
d
B6
MPO(-/-)
mCherry fluorescence
GFP fluorescence
GFP fluorescence
e
***
**
% GFPhi Salmonella
MFI of GFPhi Salmonella
B6
MPO(-/-)
B6
MPO(-/-)
f
F4/80 CD11b Salmonella
g
***
% GFPhi Salmonella
CD11b
F4/80

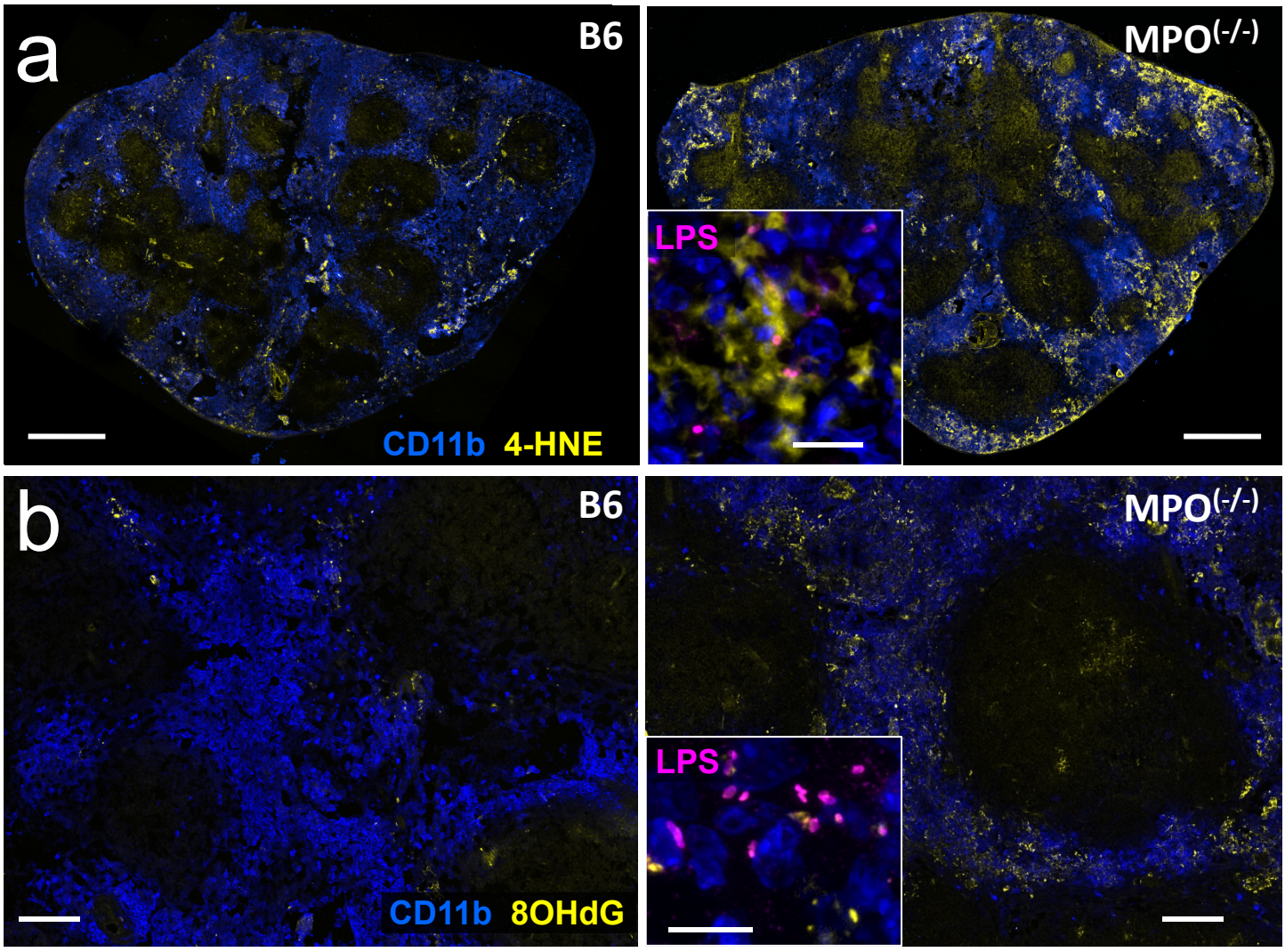
a
B6
MPO(-/-)
LPS
CD11b 4-HNE
b
B6
MPO(-/-)
LPS
CD11b 8OHdG

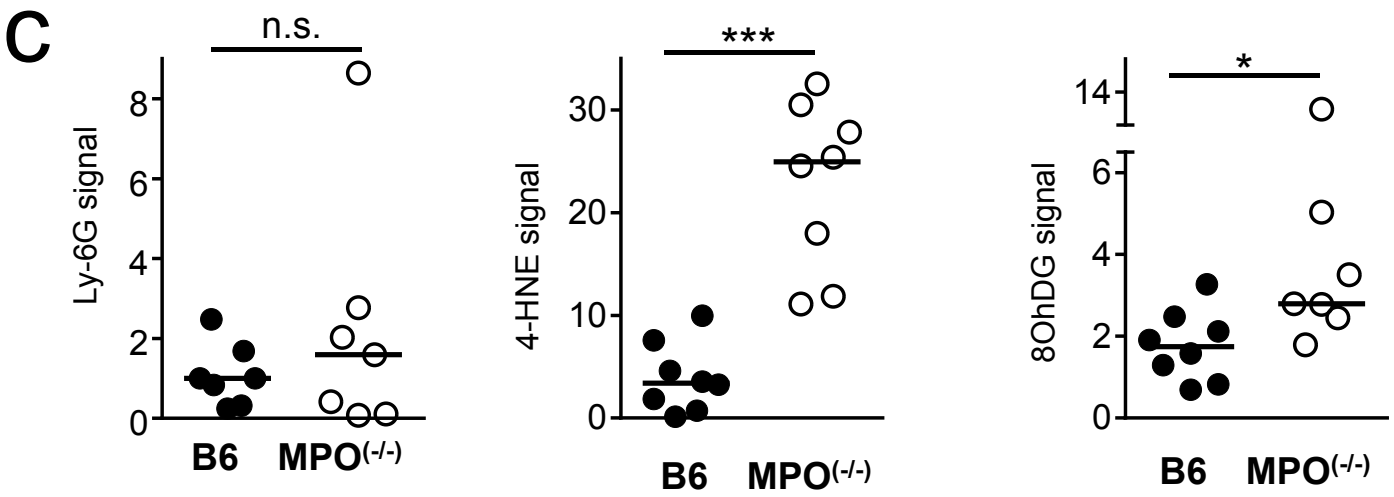
c
n.s.
***
*
Ly-6G signal
4-HNE signal
8OhDG signal
B6
MPO(-/-)

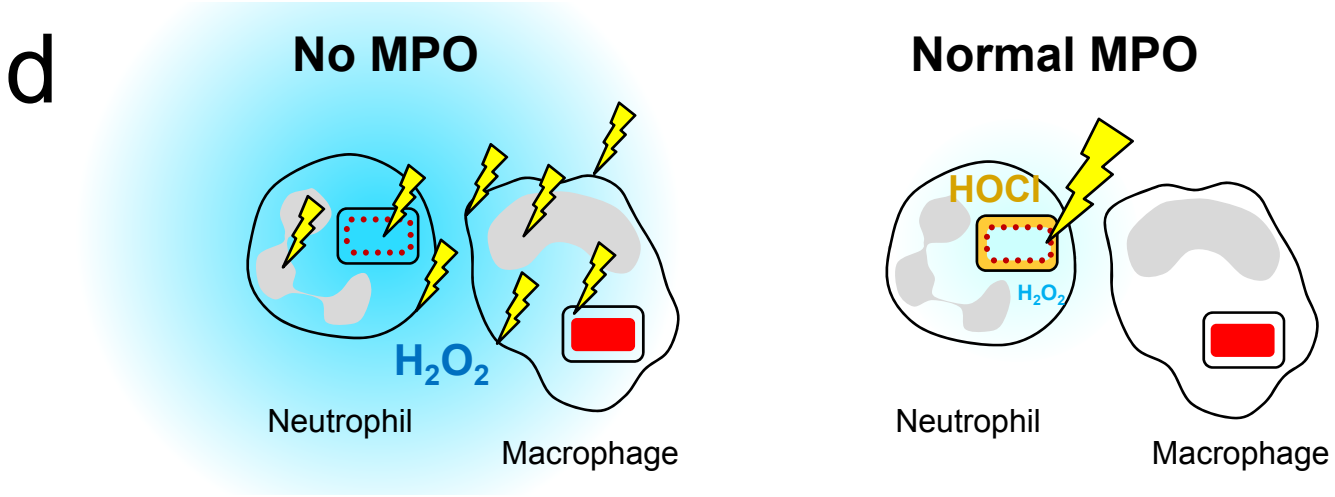
d
No MPO
Normal MPO
H2O2
HOCl
Neutrophil
Macrophage